# Regridding of remote soundings: Formulation and application to ozone profile comparison

Yasmine Calisesi[1]
International Space Science Institute, Bern, Switzerland

Vincent T. Soebijanta[2]
Belgian Institute for Space Aeronomy, Uccle, Belgium

Roeland van Oss
Royal Netherlands Meteorological Institute, De Bilt, Netherlands

Received 22 April 2005; revised 12 August 2005; accepted 1 September 2005; published 6 December 2005.

[1] One of the difficulties arising when intercomparing independent measurements of atmospheric constituent profiles consists in homogenizing their respective profile coordinates in order to allow quantitative comparison results. Special care should be devoted in particular to the homogenization of remote sensor measurements, those being indeed intricately bound to their respective numerical grids through discretization rules implied for the evaluation of the retrieval algorithms. Recently, a method of intercomparing remote sounders while allowing for different observational characteristics was proposed by Rodgers and Connor (2003). However, at the time of publication, application of this method was restricted to comparisons of identical state vectors. We propose to relax this condition by the use of linear transformation functions to homogenize the products of independent retrievals. We combine this technique with the Rodgers and Connor procedure to compare independent ozone profile measurements by the Global Ozone Monitoring Experiment (GOME) and a ground-based microwave radiometer (MW). Verification of the achieved results is obtained by considering a second series of MW retrievals, evaluated directly on the GOME numerical grid.

**Citation:** Calisesi, Y., V. T. Soebijanta, and R. van Oss (2005), Regridding of remote soundings: Formulation and application to ozone profile comparison, *J. Geophys. Res.*, *110*, D23306, doi:10.1029/2005JD006122.

## 1. Introduction

[2] There are two main difficulties associated with the intercomparison of remote soundings. The first difficulty is related to the essence of this data, these being indeed the result of a trade-off between information extracted from the performed measurements and some additional ("a priori") information used to constrain the retrieval results toward physically acceptable solutions. In the case of atmospheric profilers, the share of useful information actually contributed by the measurements, or the influence of other determining factors such as vertical resolution or retrieval errors, vary with altitude and depend on the observing system configuration. In intercomparison procedures, these characteristics must be taken into account in order to ensure a correct interpretation of the comparison results.

[3] The second difficulty applies more generally to any intercomparison process and resides in the inhomogeneity of the comparison data. As a matter of fact, two independent measurements of an atmospheric profile subject to intercomparison will generally be mapped onto fully different vertical grids, with different time resolutions and using different units. In the case of remote sounders, the homogenization of independently retrieved state vectors is hampered by the intricate bond linking the retrieval results to their respective numerical evaluation grids. This is induced by the discretization of the retrieval algorithms and the associated use of explicitly or implicitly implied averaging or sampling rules for the evaluation of the forward and inverse retrieval models. Accurate intercomparisons of remote sounders require in addition the homogenization of auxiliary retrieval products, such as averaging kernels or covariance matrixes, for which an adequate formalism has to be developed. Although seemingly trivial, the problem of the homogenization of remote sounding measurements thus still deserves consideration in order to achieve reliable comparison results.

[4] The first problem was recently addressed by *Rodgers and Connor* [2003], who proposed to account for differing observing system characteristics by eliminating identified bias contributions from the obtained comparison results. These contributions are commonly assimilated to the re-

[1] Formerly at Institute of Applied Physics, University of Bern, Bern, Switzerland.
[2] Deceased 14 November 2003.


0148-0227/05/2005JD006122$09.00

trieval smoothing error [*Rodgers*, 1990; *Tsou et al.*, 1995; *Connor et al.*, 1995] and arise from (1) the use of different a priori information with different observing systems, (2) the use of different optimization rules in the inverse models, and (3) the measurement of different subspaces of the state space by different observation systems. Correction for these differing characteristics is achieved by adjusting the retrieval products to unified retrieval rules and constraints. This approach is essential to a better interpretation of remote sounder intercomparison results. However, it was originally restricted to intercomparisons of identical state vectors. We propose to relax this condition by the use of linear transformation functions to homogenize the products of independent retrievals. The formalism applying to the regridding of independent retrieval products is introduced in section 2. An application of this formalism to the comparison of independent ozone profile measurements by the Global Ozone Monitoring Experiment (GOME) and the MeteoSwiss ground-based Stratospheric Ozone Monitoring Radiometer (SOMORA) is presented in section 3. The results of this comparison, serving also the validation of the proposed homogenization technique, are discussed in section 4.

## 2. Regridding of Retrieval Products

### 2.1. Retrieval Formalism

[5] Following the notation of *Rodgers* [2000], we denote by $\mathbf{y}$ the $m \times 1$ vector of the measured signal (''measurement vector'') and by $\mathbf{x}$ the $n \times 1$ vector of atmospheric state to be retrieved (''state vector''). For the purpose of the following discussion, we suppose that the considered state vector includes at least one set of atmospheric profile components, to which the proposed formalism will apply.

[6] The relationship between the measured signal $\mathbf{y}$ and the searched atmospheric profile $\mathbf{x}$ is provided by the forward model $\mathbf{F}(\mathbf{x})$, which describes the physics of the measurement and accounts for all known processes influencing the observed signal from its emission to its detection in the instrument. The forward model reproduces the actual measurements within accuracy $\boldsymbol{\epsilon}_\mathbf{y}$, which encapsulates both systematic and random components of the measurement and forward model errors:

$$\mathbf{y} = \mathbf{F}(\mathbf{x}) + \boldsymbol{\epsilon}_\mathbf{y} \tag{1}$$

Linearization of the forward model about some reference profile $\mathbf{x_0}$, and minimization of a cost function under the constraint of a priori information, leads to the inverse model solution [*Rodgers*, 1976]

$$\hat{\mathbf{x}} = \mathbf{x_a} + \mathbf{G_x}[\mathbf{y} - \mathbf{F}(\mathbf{x_0}) - \mathbf{K_x}(\mathbf{x_a} - \mathbf{x_0})] \tag{2}$$

where $\hat{\mathbf{x}}$ is the retrieved state vector, $\mathbf{x_a}$ is the considered a priori profile, $\mathbf{K_x}$ is the $m \times n$ Jacobian matrix of the forward model evaluated at $\mathbf{x_0}$, and $\mathbf{G_x}$ is the $n \times m$ retrieval gain matrix. The combination of the linearized version of (1) with (2) provides the relationship between the true and retrieved atmospheric profiles:

$$\hat{\mathbf{x}} = \mathbf{x_a} + \mathbf{A_x}(\mathbf{x} - \mathbf{x_a}) + \mathbf{G_x}\boldsymbol{\epsilon}_\mathbf{y} \tag{3}$$

where $\mathbf{A_x} = \mathbf{G_x}\mathbf{K_x}$ is the $n \times n$ matrix of the averaging kernels. It can be shown that the form of expression (3) applies more generally to any retrieval result, provided that when adequate $\mathbf{x_a}$ is substituted in this expression by any applying reference profile.

### 2.2. State Vector Transformation

[7] Imagine now that two independent observations of the same atmospheric profile are performed. In the most general case, two different remote sensors will be used for these observations, so that discrepancies between the respective retrieval results could be induced by differences in both the respective systems measurements, and their retrieval models characteristics. The question of the homogenization of independent retrievals, however, amounts to that of converting the retrievals of one single instrument to another state space, all other things being equal. The focus is thus set at different state space retrievals from one single instrument, which implies that potential discrepancies would result solely from differences in the evaluation grids and units of the system forward and inverse models. As the forward model evaluation grid shall in any case be fine enough to account for the variability of the measured signal, we will in the following assume that forward model representation errors can in general be neglected. In order to derive the relationship relating to each other the products of different state space retrievals, we first need to express as a function of each other the corresponding representations of the considered state vector.

[8] In the above formalism, we named $\mathbf{x}$ the $n \times 1$ vector of the atmospheric state to be retrieved. Let us now consider two coarser representations of the state vector, $\mathbf{z}_1$ and $\mathbf{z}_2$, of length $l_1$ and $l_2$, respectively, with $l_1 < n$ and $l_2 < n$. Neglecting in a first step any possibly applying units transformation issue, we will assume that $\mathbf{x}$ and each of the $\mathbf{z}_i$s, $i = 1, 2$, are related to each other by an $n \times l_i$ linear transformation matrix, $\mathbf{W}_i$, defined such as

$$\mathbf{x} = \mathbf{W}_i\mathbf{z}_i + \boldsymbol{\epsilon}_{\mathbf{W}_i}\mathbf{x} \tag{4}$$

and for which $\mathbf{z}_i$ should satisfy

$$\mathbf{z}_i = \mathbf{W}_i^*\mathbf{x} \tag{5}$$

where $\mathbf{W}_i^*$ is a generalized pseudo inverse of $\mathbf{W}_i$ [*Moore and Nashed*, 1973; *Penrose*, 1955; *Rodgers*, 2000], and $\boldsymbol{\epsilon}_{\mathbf{W}_i}\mathbf{x} = (\mathbf{I} - \mathbf{W}_i\mathbf{W}_i^*)\mathbf{x}$ is the error induced by the interpolation rule on the reconstructed fine grid vector.

[9] It follows from (4) and (5) that $\mathbf{z}_1$ and $\mathbf{z}_2$ are related to each other by the $l_1 \times l_2$ transformation $\mathbf{W}_{12}$, such as

$$\mathbf{z}_1 = \mathbf{W}_{12}\mathbf{z}_2 + \boldsymbol{\epsilon}_{\mathbf{W}_{12}}\mathbf{x} \tag{6}$$

with $\mathbf{W}_{12} = \mathbf{W}_1^*\mathbf{W}_2$ and $\boldsymbol{\epsilon}_{\mathbf{W}_{12}} = \mathbf{W}_1^*(\mathbf{I} - \mathbf{W}_2\mathbf{W}_2^*)$, or, inversely,

$$\mathbf{z}_2 = \mathbf{W}_{21}\mathbf{z}_1 + \boldsymbol{\epsilon}_{\mathbf{W}_{21}}\mathbf{x} \tag{7}$$

with $\mathbf{W}_{21} = \mathbf{W}_2^*\mathbf{W}_1$ and $\boldsymbol{\epsilon}_{\mathbf{W}_{21}} = \mathbf{W}_2^*(\mathbf{I} - \mathbf{W}_1\mathbf{W}_1^*)$.

[10] S. Migliorini et al. (Quasi-optimal assimilation of remote sounders: Formulation, submitted to *Quarterly*

*Journal of the Royal Meteorology Society*, 2005, hereinafter referred to as Migliorini et al., submitted manuscript, 2005) showed that relationships (6) and (7) also extend to nonlinear transformations of the state vector, at the condition of accounting for additional reference and bias terms which we will neglect in the present formalism for the sake of simplicity.

### 2.3. Regridding of Retrieval Products

[11] Given (4) and (5), we can now derive the relationships relating each of the coarse retrieval products $\hat{\mathbf{z}}_i$ to the fine grid result $\hat{\mathbf{x}}$. By analogy with (3), the result of a retrieval performed on a coarse numerical grid can be expressed as

$$\hat{\mathbf{z}}_i = \mathbf{z}_{\mathbf{a}_i} + \mathbf{A}_{\mathbf{z}_i}(\mathbf{z_i} - \mathbf{z}_{\mathbf{a}_i}) + \mathbf{G}_{\mathbf{z}_i}\boldsymbol{\epsilon}_{\mathbf{y}} \tag{8}$$

where $\mathbf{z}_{\mathbf{a}_i}$ is the a priori profile mapped on the $i$th coarse vertical grid, and $\mathbf{G}_{\mathbf{z}_i}$ and $\mathbf{A}_{\mathbf{z}_i} = \mathbf{G}_{\mathbf{z}_i}\mathbf{K}_{\mathbf{z}_i}$ are the gain and averaging kernels matrixes evaluated on the same numerical grid. Note that $\boldsymbol{\epsilon}_{\mathbf{y}}$ is maintained as in (3), as the forward model and measurement errors have been supposed to remain unaffected by the choice of the retrieval grid.

[12] Multiplication of equation (3) with $\mathbf{W}_i^*$, and term-to-term identification with (8) using (5), leads to the relationship

$$\hat{\mathbf{z}}_i = \mathbf{W}_i^*\hat{\mathbf{x}} \tag{9}$$

when

$$\mathbf{A}_{\mathbf{z}_i}\mathbf{W}_i^* = \mathbf{W}_i^*\mathbf{A}_{\mathbf{x}} \text{ i.e. } \mathbf{A}_{\mathbf{z}_i} = \mathbf{W}_i^*\mathbf{A}_{\mathbf{x}}\mathbf{W}_i \tag{10}$$

and

$$\mathbf{G}_{\mathbf{z}_i} = \mathbf{W}_i^*\mathbf{G}_{\mathbf{x}} \tag{11}$$

With $\mathbf{A}_{\mathbf{x}} = \mathbf{G}_{\mathbf{x}}\mathbf{K}_{\mathbf{x}}$ and $\mathbf{A}_{\mathbf{z}_i} = \mathbf{G}_{\mathbf{z}_i}\mathbf{K}_{\mathbf{z}_i}$, (10) and (11) also imply for the transformation of the contribution functions

$$\mathbf{K}_{\mathbf{z}_i} = \mathbf{K}_{\mathbf{x}}\mathbf{W}_i \tag{12}$$

The above relationships provide the rules for the transformation of the retrieved state vector, and that of the associated averaging kernels, retrieval gain, and Jacobian matrixes, respectively, from a fine to a coarse numerical grid. Consistently, we deduce for the inverse transformations

$$\hat{\mathbf{x}} = \mathbf{W}_i\hat{\mathbf{z}}_i + \boldsymbol{\epsilon}_{\mathbf{W}_i}\hat{\mathbf{x}} \tag{13}$$

$$\mathbf{G}_{\mathbf{x}} = \mathbf{W}_i\mathbf{G}_{\mathbf{z}_i} + \boldsymbol{\epsilon}_{\mathbf{W}_i}\mathbf{G}_{\mathbf{x}} \tag{14}$$

$$\mathbf{K}_{\mathbf{x}} = \mathbf{K}_{\mathbf{z}_i}\mathbf{W}_i^* + \mathbf{K}_{\mathbf{x}}\boldsymbol{\epsilon}_{\mathbf{W}_i} \tag{15}$$

where $\boldsymbol{\epsilon}_{\mathbf{W}_i} = (\mathbf{I} - \mathbf{W}_i\mathbf{W}_i^*)$ as in (4), and

$$\mathbf{A}_{\mathbf{x}} = \mathbf{W}_i\mathbf{A}_{\mathbf{z}_i}\mathbf{W}_i^* + \boldsymbol{\epsilon}_{\mathbf{A}_i} \tag{16}$$

where $\boldsymbol{\epsilon}_{\mathbf{A}_i} = \mathbf{A}_{\mathbf{x}} - \mathbf{W}_i\mathbf{W}_i^*\mathbf{A}_{\mathbf{x}}\mathbf{W}_i\mathbf{W}_i^*$ is the error affecting the reconstructed fine grid averaging kernels.

[13] Relationships (9)–(16) illustrate the fact that, provided the transformation matrixes, the transformation of a fine retrieval result into a coarse one is always possible, while the reverse operation can in general only be achieved within the range of some interpolation error $\boldsymbol{\epsilon}_{\mathbf{W}_i}$. Identification of the right-hand sides of relations (13)–(16) for the different indices $i$ leads us to the searched expressions for the transformation of retrieval products across independent numerical grids

$$\hat{\mathbf{z}}_1 = \mathbf{W}_{12}\hat{\mathbf{z}}_2 + \boldsymbol{\epsilon}_{\mathbf{W}_{12}}\hat{x} \tag{17}$$

$$\mathbf{K}_{\mathbf{z}_1} = \mathbf{K}_{\mathbf{z}_2}\mathbf{W}_{21} + \mathbf{K}_{\mathbf{x}}\boldsymbol{\epsilon}_{\mathbf{W}_{12}}^* \tag{18}$$

$$\mathbf{G}_{\mathbf{z}_1} = \mathbf{W}_{12}\mathbf{G}_{\mathbf{z}_2} + \boldsymbol{\epsilon}_{\mathbf{W}_{12}}\mathbf{G}_{\mathbf{x}} \tag{19}$$

$$\mathbf{A}_{\mathbf{z}_1} = \mathbf{W}_{12}\mathbf{A}_{\mathbf{z}_2}\mathbf{W}_{21} + \mathbf{W}_1^*\boldsymbol{\epsilon}_{\mathbf{A}_2}\mathbf{W}_1 \tag{20}$$

where $\boldsymbol{\epsilon}_{\mathbf{W}_{12}}^* = (\mathbf{I} - \mathbf{W}_2\mathbf{W}_2^*)\mathbf{W}_1$ and $\boldsymbol{\epsilon}_{\mathbf{W}_{12}} = \mathbf{W}_1^*(\mathbf{I} - \mathbf{W}_2\mathbf{W}_2^*)$ as in (6).

[14] Using (8), we find that the difference $\boldsymbol{\delta}$ between two independent retrieval results, $\hat{\mathbf{z}}_1$ and $\hat{\mathbf{z}}_2$, where $\hat{\mathbf{z}}_2$ is transposed to the state space of $\hat{\mathbf{z}}_1$ using $\hat{\mathbf{z}}_1' = \mathbf{W}_{12}\hat{\mathbf{z}}_2$, has for covariance

$$\begin{aligned}\mathbf{S}_{\delta} = {} & (\mathbf{A}_{\mathbf{z}_1} - \mathbf{I}_1)^T\mathbf{S}_{\mathbf{a}_1}(\mathbf{A}_{\mathbf{z}_1} - \mathbf{I}_1) \\ & + \mathbf{W}_{12}^T(\mathbf{A}_{\mathbf{z}_2} - \mathbf{I}_2)^T\mathbf{S}_{\mathbf{a}_2}(\mathbf{A}_{\mathbf{z}_2} - \mathbf{I}_2)\mathbf{W}_{12} \\ & + \mathbf{S}_{\mathbf{z}_1} + \mathbf{W}_{12}^T\mathbf{S}_{\mathbf{z}_2}\mathbf{W}_{12}\end{aligned} \tag{21}$$

where $\mathbf{S}_{\mathbf{a}_1}$ and $\mathbf{S}_{\mathbf{a}_2}$ are the a priori covariance matrixes of retrievals 1 and 2, respectively, $\mathbf{S}_{\mathbf{z}_1} = \mathbf{G}_{\mathbf{z}_1}{}^T\mathbf{S}_{\mathbf{y}_1}\mathbf{G}_{\mathbf{z}_1}$ and $\mathbf{S}_{\mathbf{z}_2} = \mathbf{G}_{\mathbf{z}_2}^T\mathbf{S}_{\mathbf{y}_2}\mathbf{G}_{\mathbf{z}_2}$ are the systems respective measurements error covariances, and $\mathbf{I}_1$ and $\mathbf{I}_2$ are the identity matrixes in the corresponding state spaces.

### 2.4. Practical Implementation

[15] Expressions (17)–(20) relate with each other the products of retrievals evaluated on different numerical grids, all other things being equal. They thus provide a mean of homogenizing independent retrieval results, under the condition that their error terms remain vanishingly small and can therefore be neglected in the transformation procedure. This condition constitutes indeed the main caveat of the discussed approach but can be fulfilled by an appropriate choice of $\mathbf{W}_i$s and $\mathbf{W}_i^*$s, for instance following *Rodgers* [2000] and Migliorini et al. (submitted manuscript, 2005).

[16] Under the most favorable conditions, that is, when the levels of one of the two considered numerical grids constitute a subset of the other grid's levels, expressions (9)–(16) can be used directly. In the general case, however, expressions (17)–(20) will apply. In this case, the construction of a finer, superset grid is required for the definition of the $\mathbf{W}_i$s. As in the work by Migliorini et al. (submitted manuscript, 2005), the superset grid will then to the mini-

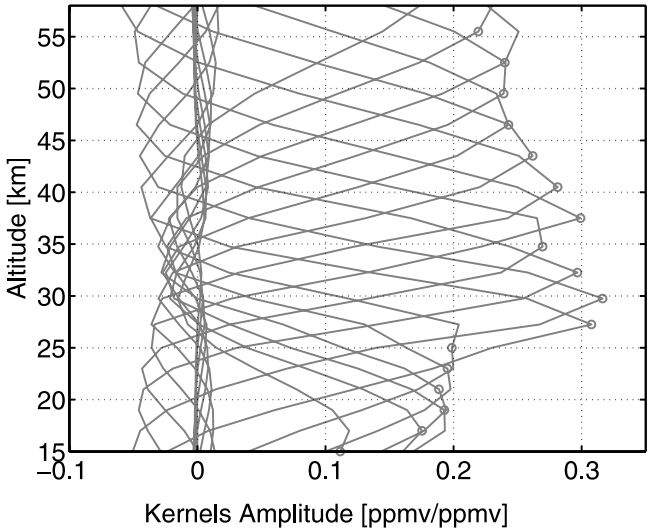


**Figure 1.** Averaging kernels for the SOMORA ozone VMR retrievals. The nominal height of each kernel is marked by a circle.

mum be defined as the superposition of the two original numerical grids.

[17] In the practice also, the homogenization of independent retrieval results will generally imply some unit conversion for at least one of the retrieved state vectors. This presupposes the definition of a diagonal unit conversion matrix $\mathbf{U}_i$, to be applied to the yet untransformed state vector with original units $\tilde{\mathbf{z}}_i$. If this case applies, the unit transformation procedure can be accounted for in the above formalism by replacing the $\mathbf{z}_i$s by $\mathbf{z}_i = \mathbf{U}_i\tilde{\mathbf{z}}_i$ in equations (4)–(7) and consistently adjusting the results of section 2.3.

## 3. Application: Intercomparison of Ground- and Satellite-Based Ozone Profile Observations

[18] We used the above formalism combined with the method proposed by *Rodgers and Connor* [2003] to compare independent ozone profile observations performed during 2000 with the satellite-borne Global Ozone Monitoring Experiment (GOME) [*Burrows et al.*, 1999] and the ground-based millimeter-wave Stratospheric Ozone Monitoring Radiometer (SOMORA) [*Calisesi*, 2003]. Both instruments provide measurements of the stratospheric ozone profile, though on different vertical grids and in different units.

### 3.1. Instrument Characteristics

[19] SOMORA provides quasi-continuous observations of the stratospheric and mesospheric ozone volume mixing ratio (VMR) profile. The instrument monitors the rotational transition line of ozone at 142.175 GHz. Information about the species vertical distribution is extracted from the recorded pressure-broadened emission spectra using an iterative optimal estimation retrieval algorithm [*Rodgers*, 1976; *Calisesi*, 2000]. The retrieved state vector consists of 29 ozone profile components, complemented with four auxiliary observational parameters. The ozone VMR values are retrieved within fixed altitude layers of 2–20 km thickness spanning the range between the ground and 110 km altitude. The a priori profile and covariance information were computed from a series of 5-year independent microwave measurements, extended to the lower stratosphere and the troposphere using coincident Brewer-Mast ozonesonde measurements [*Calisesi et al.*, 2003]. After 30 min integration time, sufficient signal-to-noise ratio is achieved in the SOMORA spectral line measurements to retrieve ozone profiles with low a priori information content between 20 and 65 km altitude. The corresponding vertical resolution, taken as the full width at half maximum of the averaging kernels (Figure 1), is of the order of 10 km in this altitude range. The SOMORA instrument was first put into operation at the Institute of Applied Physics of the University of Bern (46.95°N, 7.45°E) in August 1999, and has operated on a continuous basis since January 2000. In June 2002, the system was moved to Payerne (46.82°N, 6.95°E) where it is now operated by the Swiss Federal Institute of Meteorology and Climatology (MeteoSwiss). Since 2004, the SOMORA instrument is registered as a primary instrument of the Network for the Detection of Stratospheric Change (NDSC) (http://www.ndsc.ncep.noaa.gov/).

[20] GOME measures the solar irradiance and backscattered Earthshine radiance spectra in the 240–790 nm spectral band in a nadir-viewing geometry. Information about the vertical distribution of ozone in the stratosphere is retrieved from the 265–330 nm ozone absorption band. GOME level 2 ozone data used in the present study were processed at the Royal Netherlands Meteorological Institute (KNMI) using the Ozone Profile Retrieval Algorithm (OPERA). Like the SOMORA retrieval, this algorithm is based on an iterative optimal estimation scheme [*Rodgers*, 1976]. OPERA retrieves the profile of partial ozone column amounts within 40 layers of 1–2 km width, ranging from the ground to 0.1 hPa (~65 km). The layer boundaries are fixed in pressure, with exception of the surface and cloud top pressure levels which are adjusted to actual conditions. A priori information is provided by a hybrid ozonesonde and satellite measurement climatology [*Fortuin and Kelder*, 1998]. The a priori error covariance is obtained from an older version of the climatology. A fixed correlation matrix is used for the off-diagonal elements. With an integration time of 12 s, corresponding to a nadir spatial resolution of approximately 100 × 960 km, sufficient information is contained in the GOME measurements to retrieve ozone profiles with low a priori information content from about 15 km up to 50 km altitude. The vertical resolution of the GOME retrieval results lies between 4 and 8 km depending on altitude. The GOME averaging kernels are represented in Figure 2. GOME was launched on board the second European Remote Sensing satellite (ERS-2) onto a Sun-synchronous, near-polar orbit on 21 April 1995.

### 3.2. Data Selection

[21] The accepted coincidence and collocation criteria between the SOMORA and GOME ozone profile measurements were set to ±15 min acquisition time and ±400 km ground pixel offset, respectively. These selection criteria yielded a set of 83 coincident and collocated SOMORA

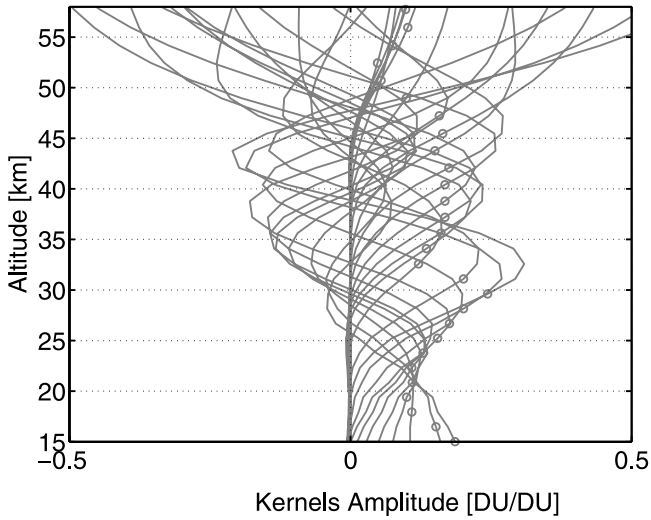


**Figure 2.** Averaging kernels for the GOME ozone profile retrievals. The kernels do not peak at their nominal altitude because of the absolute units of the retrieved profiles.

and GOME measurements acquired between 1 January and 31 December 2000.

### 3.3. Intercomparison Procedure

[22] In order to allow a quantitative comparison of the respective retrieval results, a transformation of the GOME ozone profiles to the SOMORA coordinates, or conversely, was required. We used for this purpose the formalism presented in section 2, under the assumption that the transformation errors could be neglected as discussed in section 2.4. This assumption was verified numerically, by evaluating for each comparison day the error term in the right-hand side of (17) and of its reverse relationship. The obtained typical error amplitude was contained within ±1% of the considered profile data.

[23] A sketch of the applied transformations is provided in Figure 3. We used relationships (17)–(20) and their reverse equivalents with the identities $\mathbf{W}_1 = \mathbf{W}_S$ and $\mathbf{W}_2 = \mathbf{W}_G$. $\mathbf{W}_S$ and $\mathbf{W}_G$ were both defined as four-point polynomial interpolation matrixes, and their pseudo inverses were defined as the generalized inverses $\mathbf{W}_G^* = (\mathbf{W}_G^T\mathbf{W}_G)^{-1}\mathbf{W}_G^T$ and $\mathbf{W}_S^* = (\mathbf{W}_S^T\mathbf{W}_S)^{-1}\mathbf{W}_S^T$. $\mathbf{U}$ was constructed as the diagonal matrix that converts profiles of partial ozone columns into profiles of layer-equivalent VMR values. Because of the day-to-day variability of the GOME retrieval grid, the superset vector grid was redefined anew for each comparison day.

[24] In a first step, the GOME profiles of partial ozone columns $\hat{\mathbf{z}}_G$ were converted to the superset state space using the interpolation matrix $\mathbf{W}_G$ combined with $\mathbf{U}$. Consistently with (17), the obtained fine grid ozone VMR profiles where then averaged to the SOMORA retrieval grid using the operator $\mathbf{W}_S^*$, while the GOME averaging kernels were transposed to the SOMORA retrieval coordinates using (20). The respective retrieval results were intercompared within the SOMORA state space according to *Rodgers and Connor* [2003]. The homogenized profiles were thus successively corrected for the use of different a priori information, adjusted for noniterative linear retrieval, and the GOME results were convoluted with the lower-resolution SOMORA averaging kernels using equations (10), (18), and (28) of *Rodgers and Connor* [2003]. The comparison ensemble was defined as the SOMORA a priori ensemble. The variance of the presented comparison results was compared to estimates derived from (21) or from the adjusted version of equation (30) in the work by *Rodgers and Connor* [2003]:

$$\mathbf{S}_{\delta_{12}} = \mathbf{S}_{\mathbf{z}_1} + \mathbf{A}_{\mathbf{z}_1}^T\mathbf{W}_{12}^T\mathbf{S}_{\mathbf{z}_2}\mathbf{W}_{12}\mathbf{A}_{\mathbf{z}_1} + (\mathbf{I}_1 - \mathbf{W}_{12}\mathbf{A}_{\mathbf{z}_2}\mathbf{W}_{21})^T\mathbf{A}_{\mathbf{z}_1}^T\mathbf{S}_c\mathbf{A}_{\mathbf{z}_1}(\mathbf{I}_1 - \mathbf{W}_{12}\mathbf{A}_{\mathbf{z}_2}\mathbf{W}_{21}) \quad (22)$$

An example of a simulation of the SOMORA averaging kernels using the GOME instrument is shown in Figure 4.

[25] In a second step, the SOMORA results were transposed to the GOME retrieval coordinates using the reverse transformation. A second intercomparison was then performed within the GOME retrieval space. As above, the procedure proposed by *Rodgers and Connor* [2003] was applied.

[26] Finally, a verification of the achieved comparison results was obtained by considering a second series of the SOMORA retrievals, evaluated directly on the GOME numerical grid. For the purpose of this verification, a modified version of the SOMORA retrieval program was implemented that directly outputs ozone VMR values within the GOME retrieval layers. In this case, no homogenization procedure was required other than a units conversion, allowing a direct intercomparison of the GOME and SOMORA retrieval results on their original retrieval grids. Again, the *Rodgers and Connor* [2003] procedure was applied.

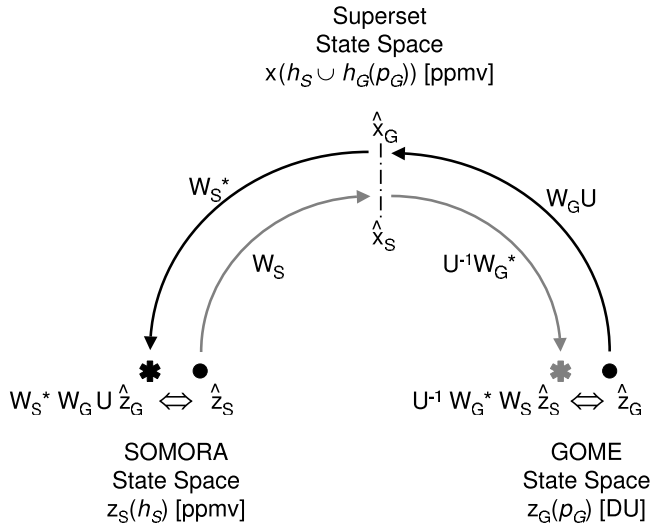


**Figure 3.** Summary of the undertaken state vector transformations. The GOME state vector is a profile of partial zone columns within fixed pressure layers, while the SOMORA results are ozone VMR profiles within fixed altitude layers. The superset state vector was chosen as an ozone VMR profile on the superposed SOMORA and GOME retrieval grids. A symmetric intercomparison was performed within each of the original retrieval state spaces.

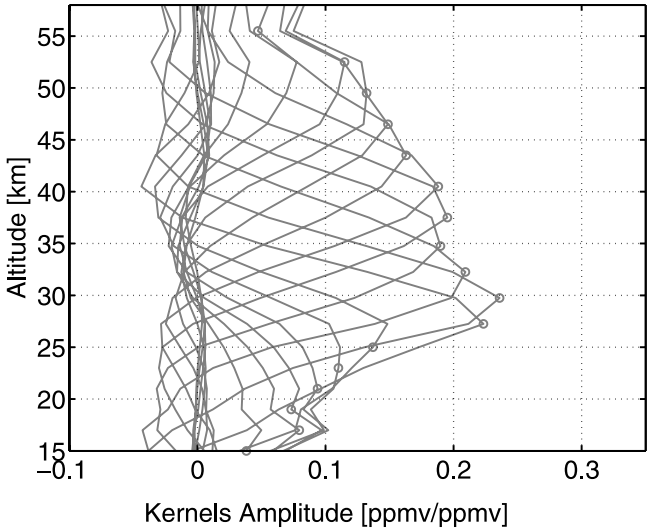


**Figure 4.** GOME averaging kernels as seen through the SOMORA instrument. The GOME kernels were transposed to the SOMORA state space, adjusted to the comparison ensemble, and convolved with the SOMORA averaging kernels following *Rodgers and Connor* [2003].

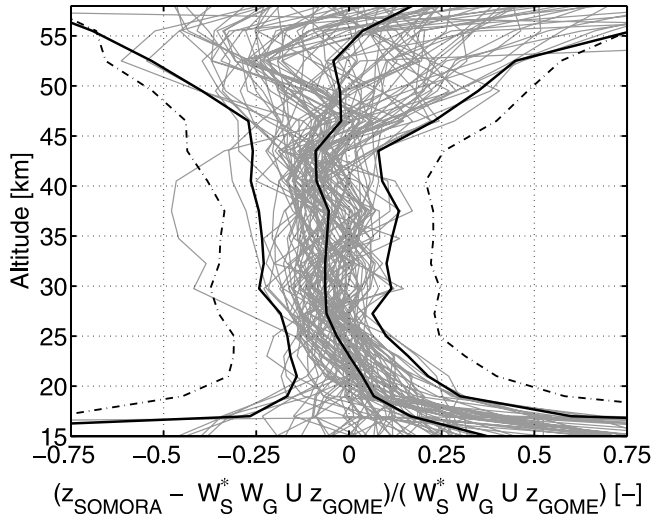


**Figure 5.** Relative difference between coincident SOMORA and GOME ozone profiles (light gray curves; GOME profiles are converted to the SOMORA state space); sample average and ±2σ width (black solid curves), where σ is the ensemble standard deviation, and expected results variance (±2σ) according to (21) (dash-dotted curves).

[27] The results of these different intercomparison series are presented in sections 4.1, 4.2, and 4.3, respectively. Validation of the proposed regridding technique is achieved by showing that no significant difference is observed between the comparison results obtained in either GOME and SOMORA original state spaces, or using the verification data set.

## 4. Results

### 4.1. SOMORA State Space

[28] Figures 5 and 6 show the results of the comparison between coincident SOMORA and GOME ozone profiles within the SOMORA state space, prior and after application of the *Rodgers and Connor* [2003] procedure. Note that while the results presented in Figure 5 are easily reproduced by simple interpolation of the GOME profiles to the SOMORA retrieval grid, the case is a bit less straightforward for Figure 6, which requires the transformation of the GOME retrieval gain and averaging kernels matrixes to the SOMORA retrieval coordinates. In the present case, a direct statistical analysis of the obtained comparison results is allowed by the time invariance of the homogenized retrieval altitude grid (SOMORA retrieval grid). The width of the obtained results distribution (±2σ, outermost solid black curves in Figures 5 and 6) can thus be compared to the expected results variance (±2σ, dash-dotted curves), estimated according to (21) and (22), respectively. For qualitative comparison with the results in the following section, the relative difference between each coincident GOME and SOMORA measurement pairs is also represented in Figures 5 and 6 (gray curves).

[29] Figure 5 reveals the existence of a systematic 2–9% bias in the altitude range 25–55 km between the SOMORA profiles and the homogenized GOME results, rapidly increasing and reversing its sign at lower and higher altitudes. This feature is characteristic for intercomparisons of remote sensors with different sensitive retrieval ranges. It reflects the progressive switch toward the respective systems' a priori profile outside of this range, that is, higher than 50 km for the GOME observations and lower than 20 km for the SOMORA measurements. The larger measurement discrepancy observed above 50 km and below 20 km goes along with an increased bias variance at those altitudes, reaching ±40% at 17 km and ±70% at 55 km (±2σ values).

[30] As expected, application of the *Rodgers and Connor* [2003] procedure (Figure 6) largely improves the agreement

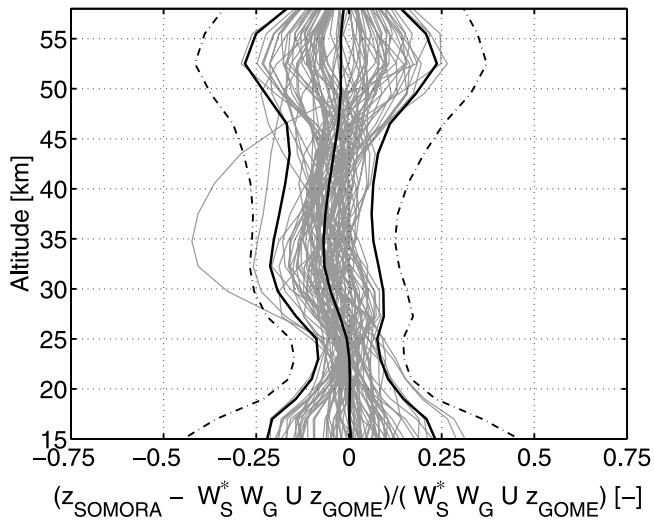


**Figure 6.** As in Figure 5 but with SOMORA and GOME results corrected for different a priori information and optimized with respect to the comparison ensemble a priori, and GOME ozone profiles convolved with SOMORA averaging kernels according to *Rodgers and Connor* [2003]. Dash-dotted curves show expected results variance (±2σ) according to (22).

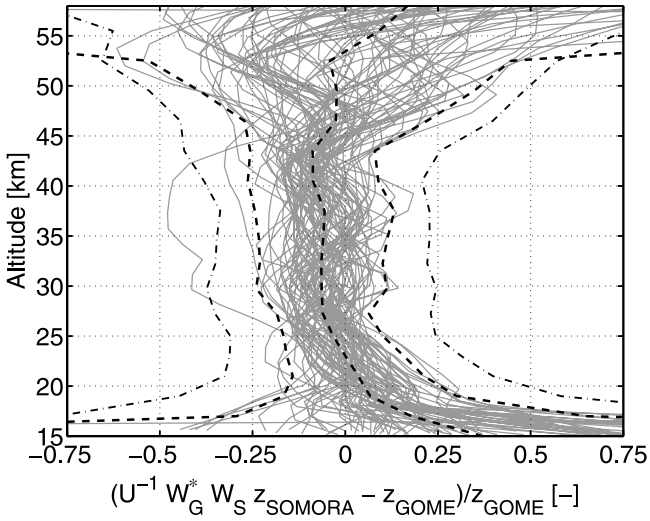


**Figure 7.** As in Figure 5, but with SOMORA profiles converted to the GOME state space. Dashed curves show sample average and ±2σ width, from gray curves interpolated to a fixed altitude grid.

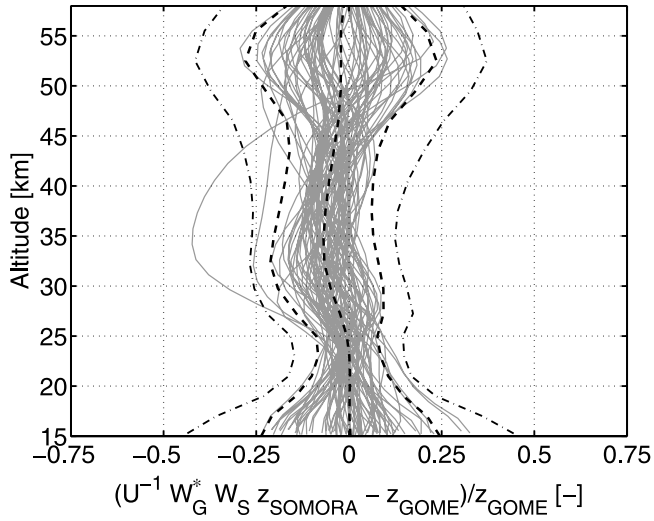


**Figure 8.** As in Figure 7, but with SOMORA and GOME profiles corrected for smoothing error as in Figure 6.

between the SOMORA and GOME retrievals. The achieved average bias lies within ±7% at all considered altitudes, with a maximum underestimation of the SOMORA ozone values with respect to GOME at the approximate altitude of the ozone VMR maximum, that is, 35 km. The obtained results variance (±2σ) is reduced to ±21% at 17 km, ±8% at 25 km, and ±23% at 55 km. In both Figures 5 and 6, the obtained results variances lie well within the values estimated using (21) and (22) (dash-dotted curves in Figures 5 and 6, respectively).

### 4.2. GOME State Space

[31] In line with the proposed method validation procedure, we expect the intercomparison results to be largely independent of the choice of the comparison state space. A first verification of this hypothesis is achieved by comparing the previous section results with those obtained within the GOME state space, that is, after converting the SOMORA results to the GOME retrieval units and vertical grid (Figures 7 and 8). In the present case, no altitude-bound statistical analysis of the obtained comparison results can be performed directly because of the day-to-day variability of the GOME retrieval altitude grid. Visual inspection of the gray curves displayed in Figures 7 and 5 and Figures 8 and 6, respectively, reveals nevertheless a good qualitative agreement between the different state space results. An insight into their quantitative agreement can be gained by considering interpolated versions of the individual bias profiles shown in Figures 7 and 8. The obtained distribution average and width (dashed curves in Figures 7 and 8) reproduce almost identically those achieved in the SOMORA state space, which tends to indicate that no significant artefact was introduced in the intercomparison results by the employed homogenization technique.

### 4.3. Verification Data Set

[32] An additional verification of the above comparison results is obtained by considering a second series of the SOMORA retrievals, evaluated directly on the GOME retrieval grid. The results obtained using this reprocessed SOMORA data set are shown in Figures 9 and 10. As above, no direct statistical analysis of the obtained comparison results can be performed along the profiles altitude grid, but indicative comparison data can be obtained by considering interpolated versions of the single comparison pairs results. Again, very good agreement is achieved with the previous section results, confirming the reliability of the proposed homogenization method.

## 5. Conclusions

[33] We proposed a simple method to regrid remote sensing observations of atmospheric constituent profiles. The method allows the homogenization of independently

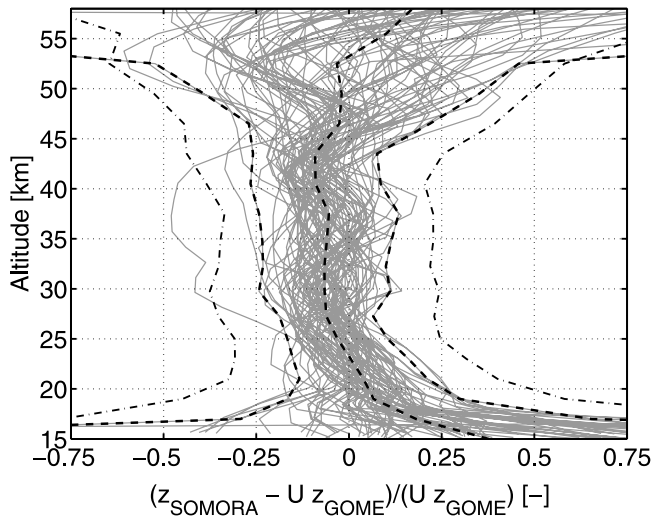


**Figure 9.** Relative difference between GOME ozone profiles and coincident SOMORA results retrieved directly on the GOME retrieval grid. Dashed curves are computed as in Figure 7.

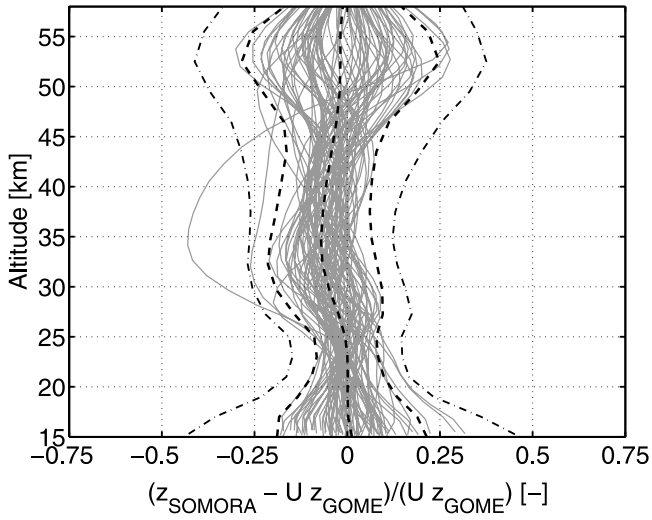


**Figure 10.** As in Figure 9, but with SOMORA and GOME profiles corrected for smoothing error as in Figure 6.

retrieved state vectors and of other associated retrieval products, without the need for altering either retrieval algorithm. By providing complete control of the undertaken transformation process, the proposed technique improves the reliability of inhomogeneous state vector intercomparison results.

[34] The proposed technique was applied to the comparison of independent remote sensing observations of the stratospheric ozone profile, performed during 2000 with the satellite-borne Global Ozone Monitoring Experiment (GOME) and the MeteoSwiss ground-based Stratospheric Ozone Monitoring Radiometer (SOMORA). After removal of smoothing error contributions, an overall ±7% average agreement was achieved in the altitude range 20–50 km between the 83 coincident SOMORA and GOME measurement pairs taken into account in the comparison. These results were verified by means of a second series of SOMORA ozone profile retrievals, evaluated directly on the GOME retrieval grid. Validation of the proposed homogenization method was achieved by comparing the reprocessed microwave data set with the original GOME profiles and by showing that no systematic differences were observed with respect to the intercomparison results obtained in each original measurement state space.

[35] **Acknowledgments.** The authors would like to thank C. D. Rodgers, S. Migliorini, A. Parrish, and K. Arzner for their very useful comments on the manuscript and for fruitful discussions about the proposed regridding technique. Many thanks also to N. Kämpfer and M. de Mazière for their support. This work was funded by PRODEX, MeteoSwiss, and the Swiss National Science Foundation under grant 200020-100153.

## References

Burrows, J. P., et al. (1999), The Global Ozone Monitoring Experiment (GOME): Mission concept and first scientific results, *J. Atmos. Sci.*, *56*, 151–175.

Calisesi, Y. (2000), The Stratospheric Ozone Monitoring Radiometer SOMORA: Data retrieval, *Res. Rep. 2000-3*, Inst. of Appl. Phys., Univ. of Bern, Bern, Switzerland.

Calisesi, Y. (2003), The Stratospheric Ozone Monitoring Radiometer SOMORA: NDSC application document, *Res. Rep. 2003-11*, Inst. of Appl. Phys., Univ. of Bern, Bern, Switzerland.

Calisesi, Y., R. Stübi, N. Kämpfer, and P. Viatte (2003), Investigation of systematic uncertainties in Brewer-Mast ozone soundings using observations from a ground-based microwave radiometer, *J. Atmos. Oceanic Technol.*, *20*, 1543–1551.

Connor, B. J., A. Parrish, J.-J. Tsou, and M. P. McCormick (1995), Error analysis for the ground-based microwave ozone measurements during STOIC, *J. Geophys. Res.*, *100*, 9283–9291.

Fortuin, J. P. F., and H. Kelder (1998), An ozone climatology based on ozonesonde and satellite measurements, *J. Geophys. Res.*, *103*, 31,709–31,734.

Moore, R. H., and M. Z. Nashed (1973), Approximations to generalized inverses, *MRC Tech. Summary Rep. 1294*, Univ. of Wis., Madison.

Penrose, R. (1955), A generalized inverse for matrices, *Proc. Cambridge Philos. Soc.*, *51*, 406–413.

Rodgers, C. D. (1976), Retrieval of atmospheric temperature and composition from remote measurements of thermal radiation, *Rev. Geophys.*, *14*(4), 609–624.

Rodgers, C. D. (1990), Characterization and error analysis of profiles retrieved from remote sounding measurements, *J. Geophys. Res.*, *95*, 5587–5595.

Rodgers, C. D. (2000), *Inverse Methods for Atmospheric Sounding*, *Ser. Atmos. Oceanic Planet. Phys.*, vol. 2, World Sci., Hackensack, N. J.

Rodgers, C. D., and B. J. Connor (2003), Intercomparison of remote sounding instruments, *J. Geophys. Res.*, *108*(D3), 4116, doi:10.1029/2002JD002299.

Tsou, J. J., B. J. Connor, A. Parrish, I. S. McDermid, and W. P. Chu (1995), Ground-based microwave monitoring of middle atmosphere ozone: Comparison to lidar and Stratospheric and Gas Experiment II satellite observations, *J. Geophys. Res.*, *100*, 3005–3016.

Y. Calisesi, International Space Science Institute, Hallerstrasse 6, CH-3012 Bern, Switzerland. (yasmine@issi.unibe.ch)

R. van Oss, Royal Netherlands Meteorological Institute, NL-3730 AE De Bilt, Netherlands.